Muon tomography: results on material identification and imaging with a large volume prototype

M. Benettoni* P. Checchia* E. Conti* F. Gonella*
S. Pesente* G. Nebbia* S. Vanini* G. Viesti*
G. Zumerle* P. Calvini† S. Squarcia† G. Bonomi‡

Abstract

The muon tomography technique, based on the multiple Coulomb scattering of cosmic ray muons, has been proposed recently as a tool to perform non-destructive assays of large volume objects without any radiation hazard. In this paper we describe the algorithms used and we show the experimental results obtained with a scanning system prototype, assembled using two large area CMS Muon Barrel drift chambers. The capability of the apparatus to produce 3D images of objects and to classify them according to their density is discussed.

Keywords : Cosmic-rays, muon tomography, volume inspection

1 Introduction

The muon tomography technique has recently been proposed as a powerful tool to inspect large volumes and to characterize composition and shape of hidden bodies [1, 2, 3, 4]. It makes use of the muon Multiple Coulomb Scattering (MCS) [5, 6]. When a muon crosses a material, its trajectory may deviate from the straight line. The projection onto a plane of the deflection angle represents the measured quantity, to be denoted by s, which has approximately a Gaussian distribution with zero mean value and root mean square σ which is related to the composition and dimension of the crossed material by

$$\sigma = \frac{13.6\text{MeV}}{\beta pc}\sqrt{\frac{x}{X_0}} \cdot \left[1 + 0.038\log(\frac{x}{X_0})\right] \approx \frac{13.6\text{MeV}}{pc}\sqrt{\frac{x}{X_0}} \qquad (1)$$

where p and βc are respectively the muon momentum and velocity, X_0 denotes the material radiation length, and x the material thickness.

Experimentally, such a technique requires the muon trajectory to be measured before and after the volume under inspection by two tracking devices (drift wire chambers, in this case).

*Universit di Padova and INFN sez. di Padova, Via Marzolo 8, 35131 Padova, Italy
†Universt di Genova and INFN sez. di Genova, via Dodecaneso 33, 16146 Genova, Italy
‡Università di Brescia, via Branze 38, 25123 Brescia, Italy, and INFN sez. di Pavia, via Bassi 6, 27100 Pavia, Italy.

In this paper, after a short mathematical introduction, we describe the tomographic prototype, which is located at the INFN National laboratories of Legnaro (Padova, Italy) and has the capability of inspecting a volume of about 11 m^3. Then, the algorithms used for the reconstruction are described and a summary of the results in terms of 3-D image reconstruction and material density classification is presented.

2 Mathematical Introduction

The projected deflections experienced by a monochromatic sample of muons of momentum p have an approximate distribution with the Gaussian width parameter σ given by eq.(1). Therefore the fairly approximate relationship

$$\sigma^2 = \frac{k^2}{p^2} t \tag{2}$$

where $k = 13.6$ MeV/c and $t = x/X_0$ can be derived.

The cosmic-ray muons at sea level have a broad momentum spectrum (from about 100 MeV/c to hundreds GeV/c) and the measurement of the momentum of each muon is a difficult task. In particular, the present configuration of the tomographic prototype does not allow the measurement of the individual muon momentum. If the momentum spectrum of the cosmic ray muons in a given environment is $f(p)$ the normalized distribution of the deviation angles s is a convolution of Gaussians having a width $\sigma(p)$ given by (2) and it can be written as:

$$\frac{dN}{ds} = \frac{1}{k\sqrt{2\pi t}} \int_0^\infty p f(p) e^{\frac{-s^2 p^2}{2tk^2}} dp. \tag{3}$$

The above integration could be performed if the spectrum $f(p)$ were known. Due to the large momentum spectrum, the distribution (3) is strongly non-Gaussian. Its second moment can anyway be computed:

$$M_2(t) \equiv < s^2 > = \int_{-\infty}^{+\infty} s^2 \frac{dN}{ds} ds = tk^2 \int_0^\infty \frac{f(p)}{p^2} dp = tk^2 < \frac{1}{p^2} > \tag{4}$$

and then it results

$$< s^2 > \propto < \frac{1}{p^2} > t \tag{5}$$

which shows a linear dependence (for equal thickness x) of the deviation angle variance $< s^2 >$ from $1/X_0$ and allows to introduce a simple estimator for the number of Radiation Lengths t crossed by N muons as

$$\hat{t}_0 = \frac{1}{N} \sum_{i=1}^{N} \frac{p_0^2 s_i^2}{k^2} \tag{6}$$

where $p_0^2 = 1/ < 1/p^2 >$. For the natural momentum spectrum at sea level $p_0 \sim 0.7$ GeV/c.

Equations (2), (3) and (6) must be modified in order to take into account the measurement error E of the scattering angle s. In particular the measurement error due to a single muon of momentum p can be parameterized as

$$E^2 = E_d^2 + \frac{k^2 t_r}{p^2} \tag{7}$$

where E_d is an intrinsic error, independent of the muon momentum, due to the detector resolution and the second term is related to the scattering on the detector material and consequently it can be described in terms of a residual thickness t_r. It must be noticed from eq.(7) that the error cannot be estimated on an event by event basis if the single muon momentum is not measured. In such a case a reasonable estimate can be:

$$E_0^2 = E_d^2 + \frac{k^2 t_r}{p_0^2}. \tag{8}$$

Then the modified equations are:

$$\sigma^2 = \frac{k^2}{p^2}(t + t_r) + E_d^2, \tag{9}$$

$$\frac{dN}{ds} = \frac{1}{\sqrt{2\pi}} \int_0^\infty \frac{p}{\sqrt{(t + t_r)k^2 + p^2 E_d^2}} f(p) e^{\frac{1}{2} \frac{-s^2 p^2}{(t+t_r)k^2 + p^2 E_d^2}} dp \tag{10}$$

and, if the individual muon momentum is not measured,

$$\hat{t}_0 = \frac{p_0^2}{k^2}(\frac{1}{N} \sum_{i=1}^{N} s_i^2 - E_d^2) - t_r. \tag{11}$$

It may be possible to measure two orthogonal projections (named $\Delta\Phi$ and $\Delta\Theta$ in the following) of the deflection angle. In principle, since the measurements are independent, it would be possible to substitute eq. (1) with two independent equations where $\sigma \to \sigma_{\Delta\Phi}$ and $\sigma \to \sigma_{\Delta\Theta}$. This would correspond to double the event statistics with respect to a sample with one measurement only. However, the absence of muon momentum measurement and its substitution with p_0 introduces a correlation between the two measurements and consequently the estimator (6) computed using two projection angles and N events is less precise than using only one projection angle and $2N$ events.

3 Experimental setup and procedure

The experimental apparatus, shown in fig. 1 and located in Legnaro (Padova, Italy) at the INFN Legnaro National Laboratories, has been described in detail in [4]. Here the main features are summarized.

The muon tomography prototype consists in two drift wire chambers, produced for the CMS experiment at CERN [7, 8], placed above and below the volume under investigation. They are supported by a structure which leaves

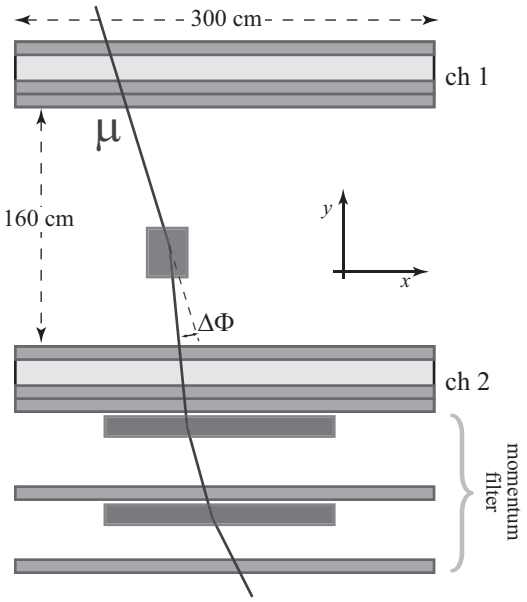

Figure 1: Scheme of the experimental setup (not to scale) in the Φ-view. The z-axis is perpendicular to the drawing plane.

an open gap of 160 cm. The two chambers have a 7.5 m^2 (3 m × 2.5 m) area and therefore a total volume of about 11 m^3 can be inspected. The muon track is measured with a single point resolution better than 200 μm. The angular resolution has a constant term on a single chamber (which depends on track inclination and corresponds to $E_d/\sqrt{2}$ in eq.(7)) of the order of 0.8 mrad for one coordinate (Φ-angle, measured in the so-called Φ-view) and of the order of 7 mrad in the other coordinate (Θ-angle). The Φ-angle has a better resolution than the Θ-angle because in the Φ-view the track is reconstructed with more points (8 in Φ and 4 in Θ) and with a larger lever arm.

Two additional Φ-view drift chambers are placed underneath the lower chamber and are interleaved by two 10 cm thick iron plates, which act as a momentum filter. The plates stop or deflect further the muon, allowing a rough determination of the muon momentum. When the inspected volume is empty, the two Fe absorbers stop muons with $p < 365$ MeV/c, for normal incidence and neglecting the chamber materials.

The data analysis of the chambers is composed by two steps. The first step consists on the reconstruction of the cosmic-ray tracks starting from the hits recorded by the chambers. Its output consists of two 2D-vectors, one for each projection (Φ and Θ view), for both the chambers and of a single vector (Φ) for the momentum filter chambers. Events having reconstructed vectors only in the uppermost chamber are also recorded to allow for possible studies of absorption effects. In the second step, the output vectors are elaborated by means of the reconstruction techniques described in the following sections, in order to provide the description of the material distribution inside the volume under investigation.

A complete simulation of the apparatus based on Monte Carlo package

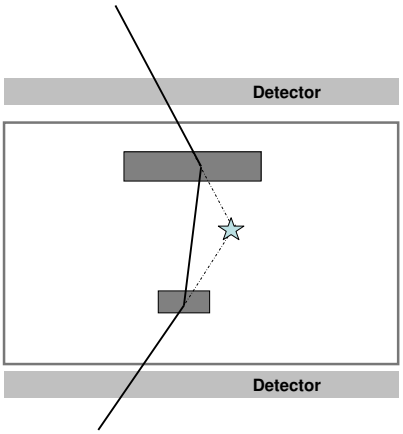

Figure 2: Example of SSPA wrong reconstruction in case of a muon crossing two material regions

Geant4 [9] is available. The simulation data agree with the experimental measurements (more details concerning simulation are available in [4]).

4 Reconstruction techniques

The simplest method to reconstruct the material distribution inside a volume is the Single Scattering Point Approximation (SSPA). It makes the assumption that the angular deviation in one projection plane (in the present case $\Delta\Phi = \Phi_{ch2} - \Phi_{ch1}$ or $\Delta\Theta = \Theta_{ch2} - \Theta_{ch1}$) is produced in a single scattering point (SP) corresponding to the intersection of the straight lines defined by the measured 2D-vectors. Then, the 3D-SP can be determined as the Point of Closest Approach (PoCA) to the 3D straight lines reconstructed from the 2D-vectors in each chamber and the amount of material t in the region around the SP can be obtained, as indicated in eq. (11), as function of $< \Delta\Phi^2 >$ (or $< \Delta\Phi^2 > + < \Delta\Theta^2 >$). The SSPA is not a good approximation for all material distributions. In particular, if muons cross several regions of high density material, the method tends to reconstruct the material in a wrong region as it is illustrated in fig. 2.

The second procedure follows a tomographic approach and is implemented in a List Mode Iterative Algorithm (LMIA). When a muon crosses different materials in sequence, the variance of the overall scattering angle depends on the total scattering length traversed $t_{tot} = \sum t_j = \sum x_j \lambda_j$ where $\lambda = 1/X_0$ is the scattering density. In the reconstruction process, the volume contained between the chambers is divided into M cubic voxels. The goal is to give an estimate of the average scattering density of each voxel. Thus, numbering the voxels by means of a single index j, the reconstruction gives values of the set $\underline{\lambda}$ whose elements are the unknowns $(\lambda_j, j = 1, ..., M)$.

The reconstruction procedure used in this study consists in an iterative optimization algorithm applied to a Maximum Log-likelihood functional and uses a 3D tomographic projector-backprojector pair, in the following referred to as the

proback pair (the proback, shortly). The projector simulates the data acquisition step and, for an assigned 3D map of the required physical quantity (the set of unknowns) generates the corresponding data. The backprojector generates a 3D map of the unknown physical quantity for a given data set and by means of the same coefficients as appearing in the projector. If the projector is a matrix, then the backprojector is represented by the transpose of that matrix. In addition, to evaluate line integrals along the muon path, the proback approximates the trajectory with the two straight segments joining the entry and exit points with the point of closest approach of the incoming and outgoing muon trajectories. In this way the proback incorporates a geometrical representation that is nicely correct, at least when the relevant contribution to the scattering occurs at a single point. An N-element dataset $\underline{s}$ consists of the data $(s_i, i = 1, ..., N)$, where each s_i is given by the angular deflection $\Delta\Phi_i$ generated by MCS along the i^{th} track (only the Φ-view is considered). The statistical distribution of s_i is given by a Gaussian probability density function

$$P_i = P(s_i|\sigma_i) = \frac{1}{\sigma_i\sqrt{2\pi}} e^{-\frac{s_i^2}{2\sigma_i^2}} \tag{12}$$

whose variance σ_i^2 is (deterministically) connected to λ by means of the following line integral

$$\sigma_i^2 = \frac{k}{p_i^2} \int_{path\ i} \lambda[r_i(l)]dl + E_i^2 \tag{13}$$

where E_i^2 is given by eq.(7).

The above integral must be evaluated along the i^{th} path given by the parametric representation $r_i(l)$. As discussed above, if the momentum information is not available for every track, it can be substituted by the appropriate average p_0. The possibility of introducing an integral over the momentum spectrum which corresponds to replace eq.(12) by eq.(10) is under study. If the collected data consist of N tracks, there are N integrals (13) which, after suitable discretization, permit to write the projector $\underline{\underline{L}}$ as an $N \times M$ matrix connecting the M-element set $\underline{\lambda}$ to the N-element set $\underline{\sigma^2}$ as

$$\sigma_i^2(\underline{\lambda}) = (\underline{\underline{L}} \cdot \underline{\lambda})_i + E_i^2 = \sum_{j=1}^{M} L_{ij}\lambda_j + E_i^2. \tag{14}$$

Every L_{ij} entry is evaluated as the product of k/p_i^2 (or k/p_0^2 in absence of momentum measurement) times the path length of the i^{th} track through the j^{th} voxel. For voxels not traversed by the track such entries are zeroed. The problem of finding, for a collected data set $\underline{s}$, the most probable $\underline{\lambda}$ map can be tackled by means of MLEM (Maximum Likelihood Expectation Maximization) strategies. In the present case it is reduced to the optimization problem of finding the minimum of the following cost function

$$\Psi(\underline{\lambda}) = \sum_{i=1}^{N} \left[\frac{s_i^2}{\sigma_i^2(\underline{\lambda})} + \ln\, \sigma_i^2(\underline{\lambda}) \right] = \sum_{i=1}^{N} \left[\frac{s_i^2}{(\underline{\underline{L}} \cdot \underline{\lambda})_i + E_i^2} + \ln[(\underline{\underline{L}} \cdot \underline{\lambda})_i + E_i^2] \right] \tag{15}$$

whose gradient $\underline{\nabla}\Psi$ can be easily evaluated. For its j^{th} component one finds

$$(\underline{\nabla}\Psi)_j = \sum_{i=1}^{N} L_{ij} \frac{(\underline{\underline{L}} \cdot \underline{\lambda})_i + E_i^2 - s_i^2}{[(\underline{\underline{L}} \cdot \underline{\lambda})_i + E_i^2]^2}. \tag{16}$$

If the individual muon momentum is not measured, in equations (14), (15) and (16) E_i must be substituted by E_0 given in eq.(8). The steepest descent algorithm [10] is used for the minimization of Ψ and an iterative procedure starting with an uniform value $\underline{\lambda}^{(0)}$ of the unknowns is performed.

The value α^* which minimizes $\Psi(\underline{\lambda}^{(0)} - \alpha\underline{\nabla}\Psi)$ is found and $\underline{\lambda}$ is updated to

$$\underline{\lambda}^{(1)} = \underline{\lambda}^{(0)} - \alpha^*\underline{\nabla}\Psi \tag{17}$$

and a new iteration is performed. The reconstruction volume is discretized into approximately $0.5 \cdot 10^6$ cubic voxels of 3 cm side. Usually about 40 iterations of the minimization algorithm are required and in the run of iterations the constraint is imposed on the λ_j entries to be greater or equal to the corresponding value for air.

The 3D reconstruction software is still in the development phase. It does not use yet the information embedded in the difference between the crossing point of the muon track in the lower chamber and the extrapolation to the same chamber of the incoming track and it does not use the Θ view with its different errors. In addition, the information coming from the momentum filter which allows to split the cosmic muon momentum spectrum in two parts is not yet implemented into a more complex but hopefully more performing algorithm.

5 Results

5.1 Imaging capability

As a first test of the imaging capability of the inspection system, the acronym INFN of our Institute made by lead bricks was used. Both the SSPA and LMIA algorithms give reasonable images (fig. 3) since the dense material is concentrated.

As a second step, the layout sketched in the left panel of fig. 4 was used. Two lead blocks ($10 \times 10 \times 20$ cm^3) and two iron blocks ($10 \times 20 \times 20$ cm^3) were placed on a support structure at a distance of about 65 cm in the vertical direction. The 3D reconstruction of this layout is reported in the right part of fig. 4 .

From both figures one can conclude that the system is able to identify correctly the position of the blocks inside the inspected volume. In particular from fig. 4 it is evident that the reconstructed scattering density for the lead is larger than for the iron blocks but it is also clear that the finite spatial resolution of the reconstruction modifies the material shape, especially in the vertical direction.

5.2 Material identification

According to the above discussion, the scattering density reconstructed on the basis of the scattering angle standard deviation should be proportional to the

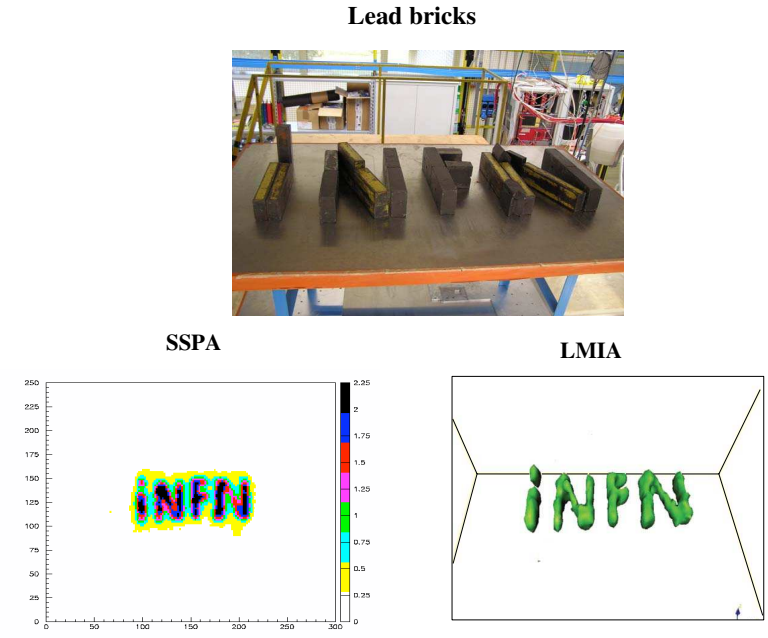

Figure 3: Imaging of the "INFN" acronym made by $10 \times 20 \times 5$ cm^3 lead bricks (top picture) performed with the SSPA (bottom left) and LMIA algorithm (bottom right).

inverse of the material radiation length. To confirm with measurements this expectation, a set of six samples made of different materials (Al, Fe, Brass, Cu, Pb and sintered W) have been placed between the chambers. Five samples were cubes of 10 cm side, while the tungsten sample was obtained by stacking up bricks of $10 \times 10 \times 4$ cm^3.

In order to minimize effects due to the different thickness of the W sample and to the smearing of the reconstructed densities due to the finite spatial resolution, the integrated density of each sample was computed by summing up the reconstructed scattering densities of all the voxels contained in a volume of dimensions $21 \times 21 \times 33$ cm^3 ($7 \times 7 \times 11$ voxels) centered on the sample. The number so obtained should be proportional to the product of the material scattering density times the volume of the sample under consideration. For the tungsten sample, the number is in addition corrected for the different thickness of the sample in order to make a direct comparison with the other materials.

In Fig. 5 the reconstructed normalized scattering density of the six samples is plotted versus the nominal value of the scattering density. On the same plot, the results of the reconstruction procedure applied to simulated data reproducing the same experimental situation are also reported. To make a comparison of the two runs, an overall normalization factor is applied to each data set, chosen to give the best agreement between the nominal and measured scattering densities of the three medium density samples (Fe, Brass, Cu). The statistical error on the normalized scattering density measurement is 2.8%. The measured densities

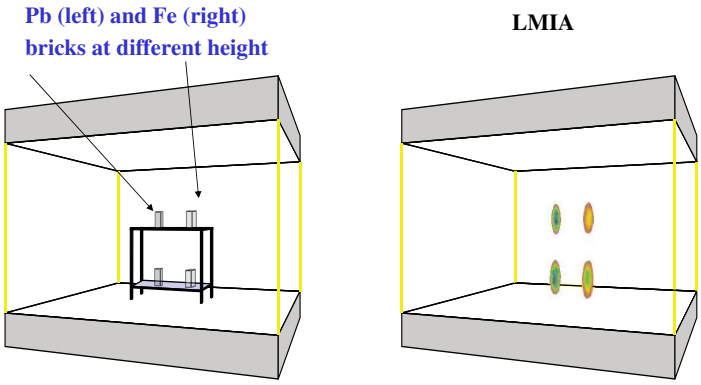

Figure 4: Left: a sketch of the layout. Pb samples are the darker ones. Right: the 3D view of the reconstructed image obtained with the iterative tomographic algorithm. The chambers have been artificially drawn in the image.

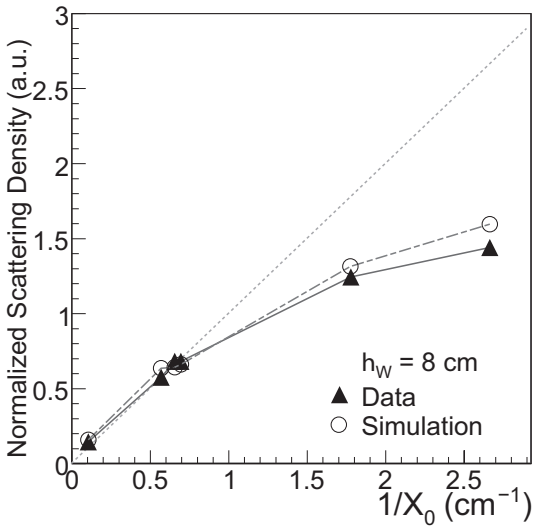

Figure 5: Correlation between the measured normalized scattering density and the inverse of the radiation length. The samples are 10 cm high, except the tungsten sample which is 8 cm high.

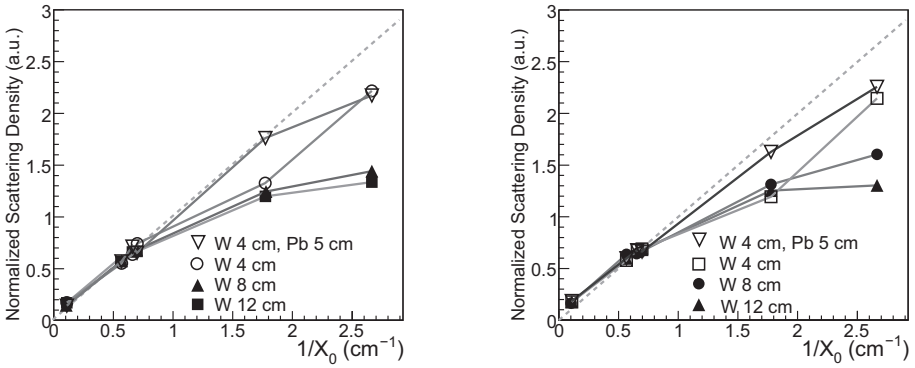

Figure 6: Correlation between the measured normalized scattering density and the inverse of the radiation length. Left plot: real data, right plot: simulated data.

do not lie on a straight line. A reduction of the measured scattering density is observed for the most dense materials. The non-linearity effect depends on the total thickness of the sample, being smaller but still present for the 4 cm W sample as it can be seen in Fig. 6

A possible explanation relies on the effects of the absorption of the low energy muons. According to equation (5) if the momentum is unknown the tomographic reconstruction process is based on the average p_0 which substitutes the single muon momentum p_i in equation (13). When traversing the sample material, the low momentum component of the muon spectrum is absorbed, to an extent depending on the sample nature and thickness. The effective momentum spectrum of muons used in the reconstruction of heavier materials is therefore harder than for lighter materials. Consequently, a larger value of the quantity $p_0^2 = 1/ < 1/p^2 >$ should be used in the scattering density calculation. Since the reconstruction program does not take this effect into account, the reconstructed densities for heavier materials result smaller than expected. To check the low momentum absorption hypothesis, we simulated cosmic muons crossing 10 cm thick plates. Since in the simulation the single muon momentum is known, the quantities $< (\Delta\Phi)^2 >$ and $< (p \cdot \Delta\Phi)^2 >$ could be compared. Both depend linearly on the scattering length traversed by the muons, but the first depends also on the momentum distribution of the muon sample, as shown by eq. (5), while the second should not. The results are shown in Fig. 7, normalized to replicate, for the iron plate, the Fe nominal scattering density. On the same plot the scattering densities reconstructed using the LMIA method are also shown, for a simulated run with six 10 cm cubes.

From Fig. 7 it is evident that $< (\Delta\Phi)^2 >$ values show essentially the same non linearity observed when using the LMIA reconstruction while the $< (p \cdot \Delta\Phi)^2 >$ values are perfectly linear. Apart from discrepancies of the order of 10-20% still not understood, the results shown in Fig. 7 prove unambiguously that the absorption of the low momentum muons is the main responsible for the non-linearity of the scattering density reconstruction.

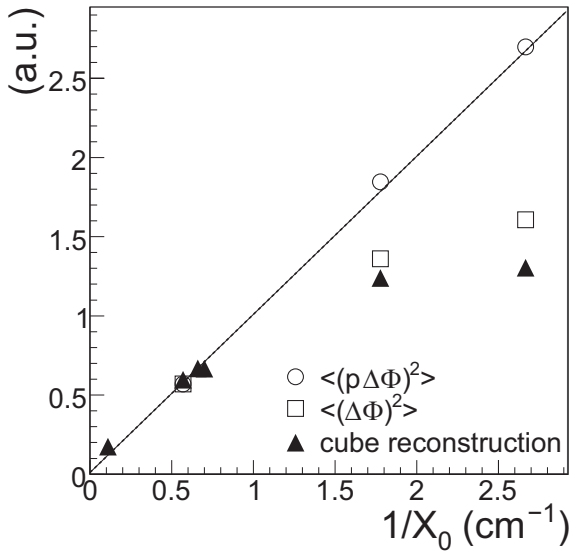

Figure 7: Comparison of the reconstructed values of the scattering densities of 10 cm cubes and the values of the quantities $< (\Delta\Phi)^2 >$ and $< (p \cdot \Delta\Phi)^2 >$ for the crossing of the same thickness of material. The three sets of data are normalized on the Fe value. The triangles correspond to the simulation of 10 cm cubes reconstructed using the LMIA method.

6 Conclusions

A large-scale prototype of a muon tomograph based on Multiple Coulomb Scattering has been built and operated. The mathematical formalism describing MCS has been included in a simple approach reconstruction (SSPA) and in a more complex tomographic iterative method based on Maximum Likelihood Expectation Maximization. In both case, however, only a simplified and preliminary version with the inclusion of a part of the whole available information was available. Results show that it is possible, in the volume under inspection, to determine different shapes and position of materials, to extract information about the average composition of objects and to discriminate among different materials. Problems in discrimination among Pb and more dense materials have been understood as due to the absorption of the low energy muon spectrum that biases the reconstruction of the scattering density. The possibility to use the absorbed particles in order to correct the effect is under study.

7 Acknowledgments

The authors thanks L. Barcellan (INFN Padova) for his valuable contribution in the maintenance of the experimental apparatus and in the data collection.

References

[1] K. R. Borozdin et al., Nature 422 (2003) 277.

[2] W. C. Priedhorsky et al., Rev. Scient. Instr. 74 (2003) 4294.

[3] L. J. Schultz et al., Nucl. Instr. and Meth. A 519 (2004) 687.

[4] S. Pesente et al., Nucl. Instrum. and Meth. A 604 (2009) 738.

[5] G.Z. Moliere, Z. Naturforsch 2a (1947) 133 and Z. Naturforsch 3a (1948) 78.

[6] H.A. Bethe, Phys. Rev. 89 (1953) 1256.

[7] The CMS Collaboration, S Chatrchyan et al., JINST 3 S08004 (2008).

[8] M. Aguilar-Benitez et al., Nucl. Instrum. and Meth. A 480 (2002), 658.

[9] S. Agostinelli et al., Nucl. Instr. and Meth. A 506 (2003) 250.

[10] W. H. Press, S. A. Teutolsky, W. T. Wetterling, B. P. Flannery Numerical Recipes in C Cambridge University Press.